2021 1st International Conference on Multidisciplinary Engineering and Applied Science (ICMEAS) | 978-1-6654-3493-5/21/$31.00 ©2021 IEEE | DOI: 10.1109/ICMEAS52683.2021.9692354

# Deep Learning-based Classification of COVID-19 Lung Ultrasound for Tele-operative Robot-assisted diagnosis

Adeyinka P. ADEDIGBA
*Department of Mechatronics Engineering,*
*Federal University of Technology, Minna, Nigeria.*
adeyinka.adedigba@futminna.edu.ng

Steve A. ADESHINA
*Department of Computer Engineering*
*Nile University, Abuja, Nigeria.*
steve.adeshina@nileuniversity.edu.ng

***Abstract*—Despite the implementation of strict COVID-19 guideline, over 300,000 healthcare workers has been infected with COVID-19 globally with over 7,000 deaths. This risk of infection and loss of vital healthcare workers can be eliminated by deploying a deep learning enhanced teleoperated robot. The robot for this study was developed by Worchester Polytechnic Institute, US, to be deployed for COVID-19 at the Nigerian National Hospital Abuja. In this paper, we develop a deep learning-based automatic classification o f l ung u ltrasound i mages f or rapid, efficient a nd a ccurate d iagnosis o f p atients f or t he developed teleoperated robot. Two lightweight models (SqueezeNet and MobileNetV2) were trained on COVID-US benchmark dataset with a computational- and memory-efficient mixed-precision training. The models achieve 99.74% (± 1) accuracy, 99.39% (± 1) recall and 99.58% (± 2) precision rate. We believe that a timely deployment of this model on the teleoperated robot will remove the risk of infection of healthcare workers.**

***Index Terms*—Deep convolution neural networks, healthcare workers, Lung Ultrasound, mixed-precision training, Robot-assisted diagnosis, Tele-medicine.**

## I. Introduction

The reverse transcriptase-polymerase chain reaction (RT-PCR) procedure has become the gold standard for diagnosing COVID-19, but the diagnosis is slow and could take hours, in addition to being in shortage of supply and low sensitivity. To this effect, other diagnosis techniques have been explored especially medical imaging such as computed tomography (CT) scans, chest x-ray (CXR) and lung ultrasound (LUS).

CT scan has been identified w ith h igh s ensitivity and accuracy, higher than RT-PCR test. The CT scan shows apparent, distinct features for COVID-19 patients such as bilateral ground-glass opacities in the lower lobes of the lungs, patchy bilateral consolidation or peripheral interstitial changes in about 97% of confirmed C OVID-19 p atients. H ence CT scan has been suggested to be more reliable than RT-PCR test [1]. Although CT scan is very accurate with high sensitivity and specificity, i t c omes w ith t he a ssociated c ost o f h igh risk of radiation exposure and high risk of COVID-19 transmission to healthy patients and healthcare workers (HCW). There is an extended protocol for disinfecting and cleaning both CT scan and the room to prevent transmission, which could take a considerable time, resulting in high downtime. Based on this associated cost and risks, the American College of Radiology recommends that CT scan should not be deployed as first-line test diagnosis of COVID-19 [2].

Further, CT scan is more expensive and unaffordable in many healthcare facilities. A cheaper imaging modality is CXR, although with less sensitivity. The following advantages of CXR imaging for the detection of COVID-19 were identified in [3]: firstly, CXR is considered the standard healthcare equipment; thus, it is readily available and accessible in many hospitals. Secondly, unlike CT scans, portable CXR systems are available; consequently, imaging can be performed in isolation rooms. Lastly, in isolation and test centres with many patients, CXR systems can allow for the rapid triaging of patients. However, compared to CT scan, it is more challenging to observe the specific features of COVID-19 infected lungs from CXR [4].

Aside from CXR, another relatively cheaper imaging modality is LUS which can be used at point-of-care in the emergency department as well as intensive care unit [5]. Deployment of LUS can significantly speed up diagnosis time, reduce crowding and congestion of the emergency department. Further advantages of LUS include portability, bedside diagnosis, zero radiation (unlike CT scan and CXR), and ease of prognosis [5]. Further, like a CT scan, LUS can identify sublime changes in the histopathologic features of superficial lung tissues peculiar to COVID-19 patients. This makes LUS very desirable in the rapid diagnosis and prognosis of COVID-19 patients.

A healthy lung consists mainly of air; this is seen as incident ultrasound waves back-reflected by the visceral pleural plane, producing artifactual images characterized by horizontal reverberation on the pleural line, usually referred to as A-line. In abnormal lungs, the ratio between air, tissue, fluid and other biological components is reduced. Hence, the lung is no longer seen as a complete spectacular reflector, but other localized vertical artefacts begin to appear corresponding to the alteration of the subpleural tissues in the lungs. In this case, the artefacts appear as B-lines of varying heterogeneous appearance [6].

Clinical findings of COVID-19 features on LUS are shown in stages: first, the pulmonary appears to contain a patchy

distribution of interstitial artifactual signs such as single or confluent vertical artefacts that extend to multiple lung areas surface as the infection progress. Further, the appearance evolved to small subpleural consolidation with associated areas of white lungs, which finally developed towards insufficient respiration. These appearances are seen as several B-lines scattered in the image; the higher the number of B-lines, the more acute the infection severity [7].

In the proceeding paragraphs, we have established the practicality of LUS in the early detection of COVID-19. In this paper, we take full advantage of LUS portability to present a method of minimizing the infection rate of healthcare workers. According to Udwadia *et al.* [8] over 3,000 HCW were infected with COVID-19 within the first three month. Although more sophisticated protocols have been put in place, over 300,000 HCW has been infected globally, with more than 7,000 death [9]. This death rate presents a global shortage of HCW, which could breed more challenges if not curtail.

Due to the portability of LUS, a low-cost teleoperated robotic LUS scanning platform was developed by Tsumura *et al.* in [10]; this robot was brought to Nigeria via the Africa University of Science and Technology, Abuja to be deployed for COVID-19 diagnosis at the Nigerian National Hospital, Abuja. For now, the teleoperated robot required an expert sonographer and radiology to interpret the acquired images. The speed of diagnosis and fatigue of human radiologists present a bottleneck in this operation, leading to congestion of test centres and misdiagnosis. Hence, we present the automatic classification of LUS images using deep learning techniques for the teleoperated robot's higher efficiency. A successful deployment of a deep learning enhanced teleoperated robot will eliminate the threat of infection of HWC workers by allowing diagnosis and prognosis to be performed at a safe distance. The diagnosis can be performed faster, and results generated within seconds; this will reduce wait periods and decongest test centres.

Therefore, in this paper, we developed a deep learning-based model for the automatic classification of COVID-19 LUS images. The model was developed to be executed on low-specification computers using computational- and memory-efficient mixed-precision training algorithm. This will prevent additional computational burden on the computer which concurrently run the robotic software and the deep learning software. The rest of the paper is organized as follows: the review of related work both on robotic and deep learning-based COVID-19 classification from LUS images is presented in Section II, the robotic design, as well as deep learning model, is presented in Section III; finally, the result and discussion of the result are presented in Section IV.

## II. Review of Related Works

The review of related works is presented here under two subsections. We reviewed related works in the design of robot-assisted diagnosis and also research efforts towards an automatic diagnosis of COVID-19 patients from LUS images.

### *A. Development of Robot-assisted Diagnosis*

Robots have been deployed in different fields due to their ability to handle adverse hazardous environments, speed of operation, ease of repeatability and precision. In medical applications, robot assistance has seen increasing research interest over the years. In this subsection, we focus on robot-assisted ultrasound.

The design of robot-assisted ultrasound began in late 1990, with the intent of designing a more user-friendly interface to enhance sonographers [11]. Since then, robot-assisted ultrasound has seen several developments such as human-operator corporation control, autonomous operation control and tele-operative robots. Although some of these earlier robots were designed for general medical operation, several researchers present robots optimized explicitly for a particular operation with specific dexterity and constraint needed to carry out the task.

Examples of operation-specific designs include [12] who designed an ultrasound-guided robot for breast biopsies, a robot-assisted carotid artery tracking was presented in [13] and robot-assisted abdominal ultrasound measurement was presented in [14]. A more detailed review of robot-assisted ultrasound is presented in [15]. Apart from the robot used in this work, another robotic-assisted ultrasound specifically for COVID-19 was developed in [16] where a 5G-based teleoperated robot-assisted ultrasound was developed for cardiopulmonary assessment of COVID-19 patients. The robot is based on a multi-link robot arm which is not suitable for lung ultrasound. The advantage of the robot used in this work is its simplicity of design optimized for low-income regions.

### *B. Development of automatic COVID-19 diagnosis from LUS*

The primary aim of this work is to develop a deep learning-based automatic diagnosis of COVID-19 from the LUS image. Hence, a brief review of related works reported in the literature is presented herewith.

A deep learning framework for automatic diagnosis of patients at Point-of-care has been presented in various form in the literature. A deep learning model for the classification of point-of-care lung ultrasound images was presented in [17]. The authors trained a model (called POCOVID-NET) with 1103 images extracted from 67 videos. POCOVID-NET consists of layers of VGG-16 used as feature extractors and an additional fully connected layer of 64 neurons followed by a softmax layer which classified the data into COVID, bacteria pneumonia and healthy patients. The model achieved 89% accuracy, 96% recall and 95% precision; the sensitivity, however, was 93%. The strength of this method is in careful ultrasound video frame editing. Another deep learning model based on multi-layer feature fusion is proposed in [18]. Feature fusion was achieved by direct concatenation of all layers into a fusion block, followed by two fully connected layers and a softmax layer to classify the dataset into three classes, similar to [17]. Due to limited information loss, the model performed well on the dataset with an accuracy of 91.8% and 92.5% precision. An assessment of B-line using deep learning model

was presented in [19] where an 8-layer model was trained to classify 2415 images extracted from 400 video clips of LUS. After training, a sensitivity of 93% and specificity of 96% was reported.

Most of the model reported in the literature were trained from scratch. Traning a model from scratch is computational and energy-intensive. Therefore, in this work, we explore a transfer learning approach for the automatic classification of LUS images. A similar approach was employed in [20] where a model for the classification of multi-modal medical images (CXR, CT scan and LUS) was presented. The model was significantly biased towards a particular image modality – a common pitfall for multi-modal training. Instead, we focus on LUS images for faster, less computationally intensive and accurate classification that compares favourably with models trained from scratch.

## III. Methodology

### A. Design of the Tele-operative Robotic LUS Platform

In emergency cases, such as presented by the COVID-19 pandemic, the bedside LUS in emergency (BLUE)-protocol is the widely accepted and validated protocol for diagnosing acute respiratory diseases. The protocol requires an LUS image to capture hallmark signs at ten different anterior, posterior, and lateral chest regions. These scan regions are quite difficult for a multi-link robot arm to cover. Hence the design presented in [10] used a gantry-style positioning unit that easily covers the whole chest-length as well as all the regions required by the BLUE protocol (see Fig. 1).

The gantry-style positioning unit is less costly to fabricate and is well suited for low-resource regions than robotic arms. Besides, it provides the robot with manoeuvrability and reachability to scan the hemithoracic regions with minimal risk of colliding with the patient's body. The robot also features a passive end-effector unit with a spring-based safety mechanism that prevents the probe from exerting excessive force on the patient. Lastly, three cameras and a two-way microphone are attached to the robot for teleoperation reasons and real-time communication with the patient.

### B. Dataset

The deep learning employed in this work was trained on an open-access benchmark data of COVID-19 related lung ultrasound image (called COVIDxUS)[1] collected and curated by [21]. The dataset contains 174 videos of lung ultrasounds from COVID patients, non-COVID patients but with reported lung infection and normal LUS images for control study. The dataset was gathered from six sources: the POCUS Atlas[2], GrepMed[3], the Butterfly Network[4], Life in the Fast Lane (LITFL)[5], The Radiopaedia[6] and the CoreUltrasound[7]. The

[1]https://github.com/nrc-cnrc/COVID-US
[2]http://www.thepocusatlas.com/
[3]http://www.grepmed.com/
[4]http://www.butterflynetwork.com/
[5]http://www.litfl.com/
[6]https://radiopaedia.org/
[7]https://www.coreultrasound.com/

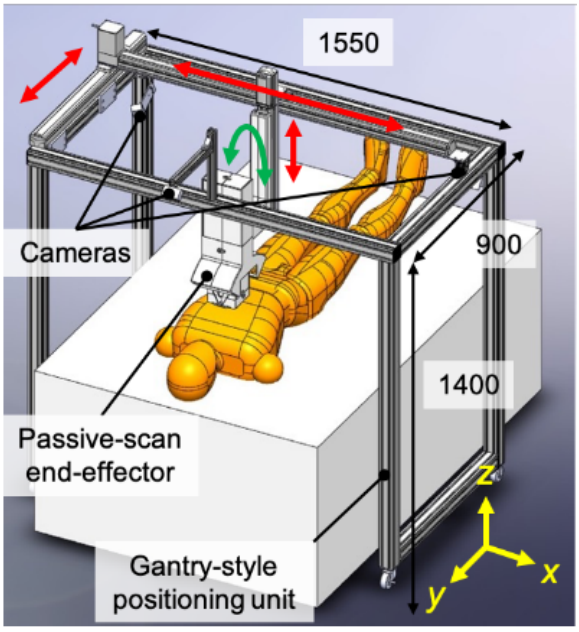


Fig. 1. The design of Robotic LUS platform consisting of gantry-style positioning unit, passive-scan end-effector and cameras [10].

distribution of videos in each data source is presented in Table I. It should be noted that both linear and convex ultrasound probes were used for data collection.

However, the goal of our robot-assisted diagnosis is to classified a LUS as COIVD-19 or non-COVID-19. Therefore, the videos of Normal and others (as shown in Table I) were merged to form the non-COVID-19 class while the COVID-19 row represents its class.

### C. Data Pre-processing

Data pre-processing techniques were carried out in this work for the following reasons: (1) the dataset contains videos of varying intensity, illumination and resolution, which must be normalized for better performance; (2) the videos must be turned to images by extracting frames from the videos; and (3) the dataset is biased towards a particular class; hence the data must be balanced for better specificity and sensitivity. Methods for achieving these objectives are presented herewith.

*1) Video Extraction and Intensity Normalization:* The videos in the dataset were recorded at an average of 30 frames per seconds, under different illumination and with different probes.

The videos were loaded from the disk, and frames were extracted from each video. Before saving to disk, histogram equalization was performed on each frame to obtain an evenly distributed intensity and intensity normalization across all the frames. In all, 7,803 images were processed.

*2) Data Augmentation:* The data augmentation was carried out to enhance our model learn invariant features from the images. Therefore, various transformations were carried out on the dataset to obtain a different variant of the same image, which will enable the model to learn invariant features

TABLE I
DATA DISTRIBUTION PER LABEL AND DATA SOURCES

| Class | ButterflyNetwork | PocusAtlas | GrepMed | LITFL | Radiopaedia | CoreUltrasound | Total |
|---|---|---|---|---|---|---|---|
| COVID-19 | 33 | 18 | 8 | 0 | 0 | 1 | 60 |
| Pneumonia | 0 | 9 | 9 | 19 | 1 | 3 | 41 |
| Normal | 2 | 5 | 3 | 3 | 1 | 1 | 15 |
| Other | 0 | 0 | 0 | 41 | 3 | 13 | 57 |

TABLE II
TABLE OF PARAMETERS FOR THE AUGMENTATION PRE-PROCESSES

| Data Augmentation | Parameter | Value(s) |
|---|---|---|
| Rotation | Rotation angle | $\pm$ [5, 10, 15] |
| Gaussian Blurring | Kernel size | 3 |
| Random Zoom | Scale | 1.3 |
| Random Lighting | Intensity | 1.4 |
| Random Warp (Affine) | Magnitude | 0.4 |

common to these images. Similarly, Gaussian blur and mild noise were simulated to make the model robust to noise. This algorithm has been developed in our previous work in [22], and the parameters of this augmentation were presented in Table II.

### *D. Mixed-precision Training*

Deep learning training is a repetitive process, usually computationally intensive, leading to high power consumption due to the longer training time. Several methods have been proposed to reduce this computational burden without negatively affecting the training accuracy. The mixed-precision training introduced in [23] was employed in this work.

The concept of mixed-precision training is as follows. While training deep learning model, in each mini-batch of data, the following computational steps are carried out: the forward-propagation, the loss computation, the weight gradient computation, the backwards-propagation of error and loss optimization. All these steps are usually carried out in 32-bit IEEE-745 single-precision floating-point numbers. However, the computation can be done 16-bit IEEE-745 half-precision floating-point number but with a loss of accuracy. To prevent this, a master copy of original weights (before weight update) is kept to retain the accuracy, whereas the forward- and backwards-propagation were carried out in half-precision. This mixed-precision ensures the accuracy is retained while speeding up the training time up to 8 times.

### *E. CNN Architecture*

For the automatic classification of COVID-19 from the LUS image, CNN architectures with smaller parameters were employed. We aim to provide a less computational and memory-intensive deep learning model with high accuracy, specificity and sensitivity. In addition, the model must have a small inference time to allow real-time diagnosis.

For this purpose, SqueezeNet and MobileNet are employed. The architecture is presented herewith.

**SqueezeNet [24]**: is a small network architecture that achieves similar performance to AlexNet on ImageNet dataset but with 50% fewer parameters. The parameter reduction was achieved by using $1\times1$ filter instead of larger filter sizes and decreasing the number of input channels to their $3\times3$ filters instead of $7 \times 7$ filters used in AlexNet. These smaller filter sizes have been shown to be an approximation of larger filter sizes in [25]. Thus, instead of using larger filters, smaller filters are repeatedly used throughout the network. The network has 421K parameters which take only 0.46MB of memory.

**MobileNetV2 [26]**: is also a small deep CNN network optimized for mobile phone. It features a reduced number of parameters (3.4M), smaller memory footprint (0.4MB) and fast inference time (75 mili-seconds). The architecture is built on two concepts: depth-wise separable convolutions and inverted residuals. The depth-wise separable convolution operation replaces a full convolution operator with a factorized version that split the convolution into two separate layers. MobileNetV2 uses $3\times3$ separable convolutions, which reduces the computational cost by nine times compared to traditional convolution. The inverted residual is similar to the residual blocks in He *et al.* [27], but the skipped connection is made between bottleneck blocks.

### *F. Overview of Experiment*

The experiments are carried out using Python programming language on an HP G8 server with 128GB RAM and 3.5GHz Intel Xenon processor. The video processing, intensity normalization and data augmentation were carried out using the Open-CV python library. Training of deep learning models was carried out using Fastai library[8].

The training parameters are as follows: the images were resized to $224 \times 224$, and a mini batch-size of 64 was used for the training. The training was carried out within 30 epoch to obtain the best performance. Adam optimizer was used with a learning rate of 0.001, the momentum of 0.98 and the L-2 norm regularization constant of 0.0001. The performance of each of the model is presented in the next section.

## IV. RESULTS AND DISCUSSION OF RESULTS

The CNN models presented in subsection III-E were fine-tuned with our dataset according to the experimental setup presented in subsection III-F. The result of this experiment is

[8]doc.fast.ai

presented herewith. Also, the performance of our models is compared with those reported in the literature.

The performance of SqueezeNet and MobileNet is presented in Table III, this performance is compared with those reported in the literature and presented in Table IV. A typical inference from SqueezeNet in real-time is presented in Fig. 2 showing the prediction probabilities for each image and the loss acquired during the process. From the Figure, the model makes accurate prediction but with high confidence (average of 0.9) and a lower loss penalty (average of 0.09). Similarly, the precision and recall rate of our models are quite high (average of 99.4%).

TABLE III
TRAINING RESULTS

| Model | Accuracy | Recall | Precision |
|---|---|---|---|
| MobileNet | 99.73 | 99.38 | 99.56 |
| SqueezeNet | 99.75 | 99.40 | 99.60 |

TABLE IV
COMPARISON OF OUR MODEL WITH THOSE REPORTED IN THE LITERATURE

| Ref | Accuracy | Precision | Recall |
|---|---|---|---|
| [17] | 89.0 | 95.0 | 96.0 |
| [18] | 91.8 | 92.5 | - |
| [19] | - | 93.0 | 96.0 |
| [28] | - | 85.7 | 1.0 |
| Our Model | 99.75 | 99.4 | 99.6 |

Lastly, the two models were tested on 1,500 LUS images. A perfect result was obtained, and the summary is presented in Fig. 4 as a confusion matrix.

The two models were trained end-to-end on the image without heavy pre-processing or feature engineering. This means the models can perform well when deployed for real-world usage without further engineering.

## V. CONCLUSION

Deep learning models for the rapid classification of COVID-19 from LUS images have been presented in this work. The developed models were based on two small parameters CNN architectures – SqueezeNet and MobileNetV2 – to be deployed for tele-operative robotic-assisted lung ultrasound. The models were trained on 7,803 images of both linear and convex ultrasound probes gathered from six different data sources. The models achieves 99.74% (± 1) accuracy, 99.39% (± 1) recall and 99.58% (± 2) precision rate. The model was tested on 1,500 ultrasound images, and it achieves a perfect classification accuracy. Further, looking at the inference of the model, it shows that the classification was performed with great confidence, lower classification cost and great accuracy. We believe that a timely deployment of this model on the tele-operative robot-assisted LUS will remove the risk of infection of healthcare workers.

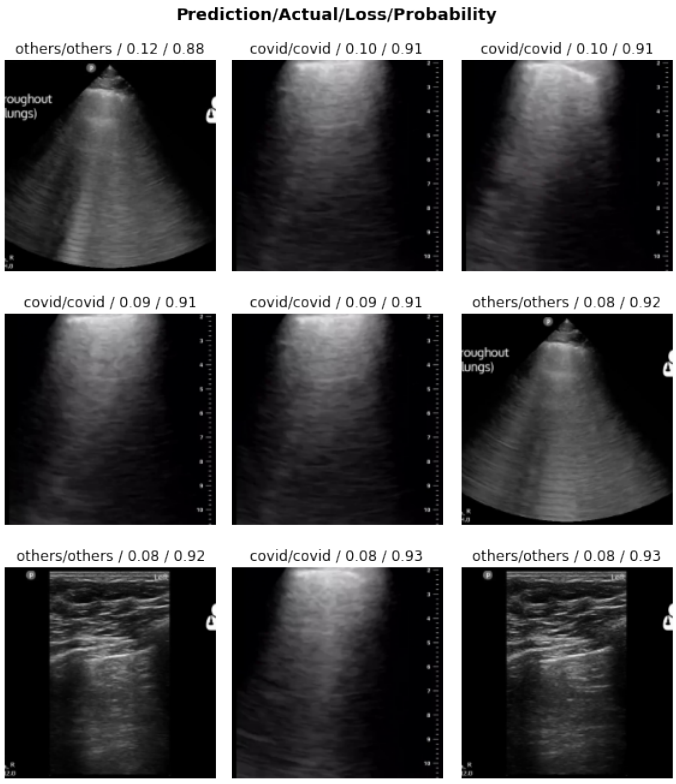


Fig. 2. Inference of deep learning-based classification

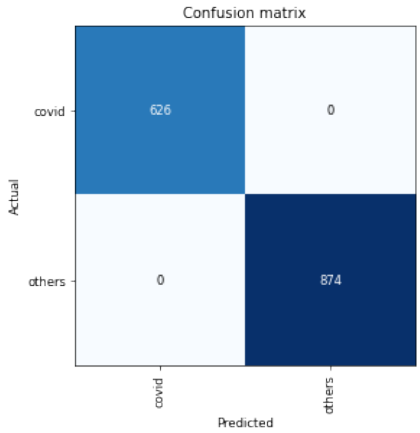


Fig. 3. Confusion Matrix of SqueezeNet on 1,500 test images

## REFERENCES

[1] G. D. Rubin, C. J. Ryerson, L. B. Haramati, N. Sverzellati, J. P. Kanne, S. Raoof, N. W. Schluger, A. Volpi, J. J. Yim, I. B. Martin, D. J. Anderson, C. Kong, T. Altes, A. Bush, S. R. Desai, O. Goldin, J. Mo Goo, M. Humbert, Y. Inoue, H. U. Kauczor, F. Luo, P. J. Mazzone, M. Prokop, M. Remy-Jardin, L. Richeldi, C. M. Schaefer-Prokop, N. Tomiyama, A. U. Wells, and A. N. Leung, "The role of chest imaging in patient management during the covid-19 pandemic: A multinational consensus statement from the fleischner society," *Radiology*, vol. 296, no. 1, pp. 172–180, 2020.

[2] R. B. Liu, V. S. Tayal, N. L. Panebianco, Y. Tung-Chen, A. Nagdev, S. Shah, E. Pivetta, P. C. Henwood, M. J. Nelson, and C. L. Moore,

"Ultrasound on the Frontlines of COVID-19: Report From an International Webinar," pp. 523–526, 2020.

[3] Y. Wang, C. Dong, Y. Hu, C. Li, Q. Ren, X. Zhang, H. Shi, and M. Zhou, "Temporal Changes of CT Findings in 90 Patients with COVID-19 Pneumonia: A Longitudinal Study," *Radiology*, vol. 296, no. 2, pp. E55–E64, 2020.

[4] A. P. Adedigba, S. A. Adeshina, O. E. Aina, and A. M. Aibinu, "Optimal hyperparameter selection of deep learning models for covid-19 chest x-ray classification," *Intelligence-Based Medicine*, p. 100034, 2021.

[5] B. Schmid, D. Feuerstein, C. N. Lang, K. Fink, R. Steger, M. Rieder, D. Duerschmied, H.-J. Busch, and D. Damjanovic, "Lung ultrasound in the emergency department-a valuable tool in the management of patients presenting with respiratory symptoms during the sars-cov-2 pandemic," *BMC Emergency Medicine*, vol. 20, no. 1, pp. 1–7, 2020.

[6] G. Soldati, A. Smargiassi, R. Inchingolo, D. Buonsenso, T. Perrone, D. F. Briganti, S. Perlini, E. Torri, A. Mariani, E. E. Mossolani, F. Tursi, F. Mento, and L. Demi, "Is There a Role for Lung Ultrasound During the COVID-19 Pandemic?" pp. 1459–1462, 2020.

[7] S. Sofia, A. Boccatonda, M. Montanari, M. Spampinato, D. D'ardes, G. Cocco, E. Accogli, F. Cipollone, and C. Schiavone, "Thoracic ultrasound and SARS-COVID-19: a pictorial essay," *Journal of Ultrasound*, vol. 23, no. 2, pp. 217–221, 2020. [Online]. Available: https://doi.org/10.1007/s40477-020-00458-7

[8] Z. F. Udwadia and R. S. Raju, "How to protect the protectors: 10 lessons to learn for doctors fighting the covid-19 coronavirus," *Medical Journal, Armed Forces India*, 2020.

[9] A. F. Goddard and M. Patel, "The changing face of medical professionalism and the impact of covid-19," *The Lancet*, vol. 397, no. 10278, pp. 950–952, 2021.

[10] R. Tsumura, J. Hardin, K. Bimbraw, A. Grossestreuer, O. S. Odusanya, Y. Zheng, J. C. Hill, B. Hoffmann, W. Soboyejo, and H. Zhang, "Tele-Operative Low-Cost Robotic Lung Ultrasound Scanning Platform for Triage of COVID-19 Patients," *IEEE Robotics and Automation Letters*, 2021.

[11] S. E. Salcudean, G. Bell, S. Bachmann, W.-H. Zhu, P. Abolmaesumi, and P. D. Lawrence, "Robot-assisted diagnostic ultrasound–design and feasibility experiments," in *International Conference on Medical Image Computing and Computer-Assisted Intervention*. Springer, 1999, pp. 1062–1071.

[12] M. K. Welleweerd, F. J. Siepel, V. Groenhuis, J. Veltman, and S. Stramigioli, "Design of an end-effector for robot-assisted ultrasound-guided breast biopsies," *International journal of computer assisted radiology and surgery*, vol. 15, no. 4, pp. 681–690, 2020.

[13] R. Nakadate, J. Solis, A. Takanishi, E. Minagawa, M. Sugawara, and K. Niki, "Out-of-plane visual servoing method for tracking the carotid artery with a robot-assisted ultrasound diagnostic system," in *2011 IEEE International Conference on Robotics and Automation*. IEEE, 2011, pp. 5267–5272.

[14] R. Nakadate, Y. Tokunaga, J. Solis, A. Takanishi, E. Minagawa, M. Sugawara, K. Niki, and A. Saito, "Development of robot assisted measurement system for abdominal ultrasound diagnosis," in *2010 3rd IEEE RAS & EMBS International Conference on Biomedical Robotics and Biomechatronics*. IEEE, 2010, pp. 367–372.

[15] D. R. Swerdlow, K. Cleary, E. Wilson, B. Azizi-Koutenaei, and R. Monfaredi, "Robotic arm–assisted sonography: Review of technical developments and potential clinical applications," *American Journal of Roentgenology*, vol. 208, no. 4, pp. 733–738, 2017.

[16] R. Ye, X. Zhou, F. Shao, L. Xiong, J. Hong, H. Huang, W. Tong, J. Wang, S. Chen, A. Cui *et al.*, "Feasibility of a 5g-based robot-assisted remote ultrasound system for cardiopulmonary assessment of patients with coronavirus disease 2019," *Chest*, vol. 159, no. 1, pp. 270–281, 2021.

[17] J. Born, G. Brändle, M. Cossio, M. Disdier, J. Goulet, J. Roulin, and N. Wiedemann, "Pocovid-net: automatic detection of covid-19 from a new lung ultrasound imaging dataset (pocus)," *arXiv preprint arXiv:2004.12084*, 2020.

[18] G. Muhammad and M. S. Hossain, "Covid-19 and non-covid-19 classification using multi-layers fusion from lung ultrasound images," *Information Fusion*, vol. 72, pp. 80–88, 2021.

[19] B. Cristiana, T. Grzegorz, K. Seungsoo, M. Katelyn, L. Rachel, M. Shaw, R. McNamara, R. Balasundar, and C. Moore, "Automated lung ultrasound b-line assessment using a deep learning algorithm." *IEEE Transactions on Ultrasonics, Ferroelectrics, and Frequency Control*, 2020.

[20] M. J. Horry, S. Chakraborty, M. Paul, A. Ulhaq, B. Pradhan, M. Saha, and N. Shukla, "COVID-19 Detection through Transfer Learning Using Multimodal Imaging Data," *IEEE Access*, vol. 8, pp. 149 808–149 824, 2020.

[21] A. Ebadi, P. Xi, A. MacLean, S. Tremblay, S. Kohli, and A. Wong, "Covidx-us - an open-access benchmark dataset of ultrasound imaging data for ai-driven covid-19 analytics," *arXiv:2103.10003*, 2021.

[22] A. P. Adedigba, S. A. Adeshina, and A. M. Aibinu, "Deep learning-based mammogram classification using small dataset," in *2019 15th International Conference on Electronics, Computer and Computation (ICECCO)*. IEEE, 2019, pp. 1–6.

[23] P. Micikevicius, S. Narang, J. Alben, G. Diamos, E. Elsen, D. Garcia, B. Ginsburg, M. Houston, O. Kuchaiev, G. Venkatesh *et al.*, "Mixed precision training," *arXiv preprint arXiv:1710.03740*, 2017.

[24] F. N. Iandola, S. Han, M. W. Moskewicz, K. Ashraf, W. J. Dally, and K. Keutzer, "Squeezenet: Alexnet-level accuracy with 50x fewer parameters and¡ 0.5 mb model size," *arXiv preprint arXiv:1602.07360*, 2016.

[25] C. Szegedy, V. Vanhoucke, S. Ioffe, J. Shlens, and Z. Wojna, "Rethinking the inception architecture for computer vision," in *Proceedings of the IEEE conference on computer vision and pattern recognition*, 2016, pp. 2818–2826.

[26] M. Sandler, A. Howard, M. Zhu, A. Zhmoginov, and L.-C. Chen, "Mobilenetv2: Inverted residuals and linear bottlenecks," in *Proceedings of the IEEE conference on computer vision and pattern recognition*, 2018, pp. 4510–4520.

[27] K. He, X. Zhang, S. Ren, and J. Sun, "Deep residual learning for image recognition," in *Proceedings of the IEEE conference on computer vision and pattern recognition*, 2016, pp. 770–778.

[28] R. Arntfield, B. Vanberlo, T. Alaifan, N. Phelps, M. White, R. Chaudhary, J. Ho, and D. Wu, "Development of a convolutional neural network to differentiate among the etiology of similar appearing pathological b lines on lung ultrasound: A deep learning study," *BMJ Open*, vol. 11, no. 3, pp. 1–9, 2021.